BIOCHEMISTRY
including biophysical chemistry & molecular biology

Article

pubs.acs.org/biochemistry

Deformation of Chlorin Rings in the Photosystem II Crystal Structure

Keisuke Saito,[†] Yasufumi Umena,[‡,§] Keisuke Kawakami,[‡] Jian-Ren Shen,[∥] Nobuo Kamiya,[‡,⊥] and Hiroshi Ishikita*[,†,§]

[†]202 Building E, Career-Path Promotion Unit for Young Life Scientists, Graduate School of Medicine, Kyoto University, Yoshida-Konoe-cho, Sakyo-ku, Kyoto 606-8501, Japan

[‡]The OCU Advanced Research Institute for Natural Science and Technology (OCARINA)/Graduate School of Science, Osaka City University, Sumiyoshi, Osaka 558-8585, Japan

[§]Japan Science and Technology Agency (JST), Precursory Research for Embryonic Science and Technology, 4-1-8 Honcho, Kawaguchi, Saitama 332-0012, Japan

[∥]Division of Bioscience, Graduate School of Natural Science and Technology/Faculty of Science, Okayama University, Okayama 700-8530, Japan

[⊥]Graduate School of Science, Osaka City University, Sumiyoshi, Osaka 558-8585, Japan

Supporting Information

ABSTRACT: The crystal structure of Photosystem II (PSII) analyzed at a resolution of 1.9 Å revealed deformations of chlorin rings in the chlorophylls for the first time. We investigated the degrees of chlorin ring deformation and factors that contributed to them in the PSII crystal structure, using a normal-coordinate structural decomposition procedure. The out-of-plane distortion of the P_{D1} chlorin ring can be described predominantly by a large "doming mode" arising from the axial ligand, D1-His198, as well as the chlorophyll side chains and PSII protein environment. In contrast, the deformation of P_{D2} was caused by a "saddling mode" arising from the D2-Trp191 ring and the doming mode arising from D2-His197. Large ruffling modes, which were reported to lower the redox potential in heme proteins, were observed in P_{D1} and Chl_{D1}, but not in P_{D2} and Chl_{D2}. Furthermore, as P_{D1} possessed the largest doming mode among the reaction center chlorophylls, the corresponding bacteriochlorophyll P_L possessed the largest doming mode in bacterial photosynthetic reaction centers. However, the majority of the redox potential shift in the protein environment was determined by the electrostatic environment. The difference in the chlorin ring deformation appears to directly refer to the difference in "the local steric protein environment" rather than the redox potential value in PSII.

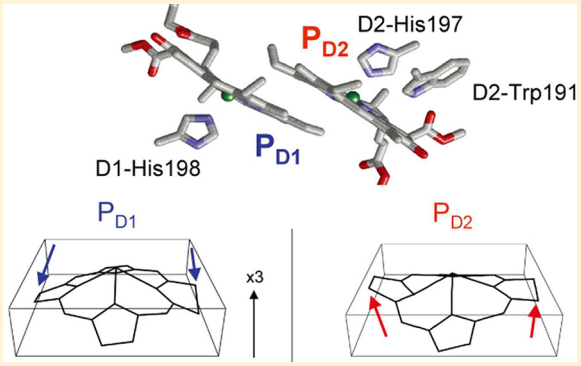

The reaction center of Photosystem II (PSII) consists of the D1−D2 heterodimer, harboring the chlorophyll *a* (Chl*a*) pair (P_{D1} and P_{D2}), the accessory Chl*a* pair (Chl_{D1} and Chl_{D2}), two forms of pheophytin *a* (Pheo*a*) ($Pheo_{D1}$ and $Pheo_{D2}$), two quinones, and two additional forms of Chl*a* [$Chl_{Z(D1)}$ and $Chl_{Z(D2)}$] as the redox-active cofactors (Figure 1). P680, which absorbs light at a wavelength of 680 nm, is formed among the four central Chl*a* molecules, P_{D1}, P_{D2}, Chl_{D1}, and Chl_{D2}. Excitation of P680 leads to the formation of the $Chl_{D1}^{\bullet+}Pheo_{D1}^{\bullet-}$ state,[1−3] followed by the $[P_{D1}/P_{D2}]^{\bullet+}Pheo_{D1}^{\bullet-}$ state. The resulting $[P_{D1}/P_{D2}]^{\bullet+}$ state serves as an electron abstractor for the oxygen-evolving cluster (OEC) and has been shown to have its positive charge predominately located in P_{D1}, with a $P_{D1}^{\bullet+}/P_{D2}^{\bullet+}$ ratio of ∼80/20.[4−7] Recently, the PSII crystal structure from *Thermosynechococcus vulcanus* was reported at a resolution of 1.9 Å.[8] The 1.9 Å structure revealed detailed geometries of not only the OEC but also other cofactors, including P_{D1} and P_{D2}, where the vinyl group is rather in plane for P_{D1} and out of the plane for P_{D2}. This may constitute one of the factors that cause breakage of the noncrystallographic 2-fold symmetry in the P_{D1}/P_{D2} Chl*a* dimer.

In addition to the structural characteristics mentioned above, the 1.9 Å structure also revealed a new feature; the chlorin rings of most of the Chl*a* molecules including the P_{D1}/P_{D2} pair are not planar.[8] In the 1.9 Å structure, electron density distributions for the magnesium atoms of Chl*a* were clearly separated from those for the chlorin rings and were located out of the ring planes in most cases. The chlorin rings were bent to various degrees depending on their environments.[8] The skeletal flexibility of chlorin rings or porphyrin rings can be imposed by the protein environment.[9] It was reported that nonplanar porphyrins are easier to oxidize and harder to reduce.[10] If this is

Received: February 16, 2012
Revised: May 7, 2012
Published: May 8, 2012

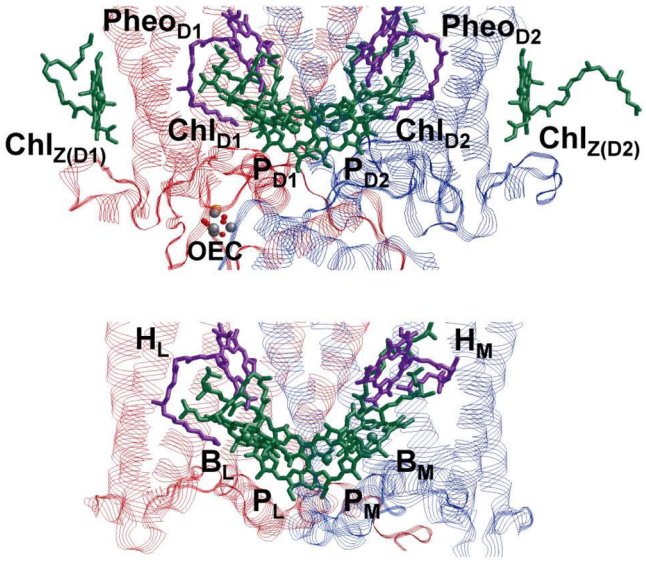

Figure 1. Chlorophylls (green) and pheophytins (purple) in the D1 (red) and D2 (blue) subunits of PSII (top) and in the L (red) and M (blue) subunits of PbRC (bottom).

the case, deformation of the chlorin rings[8] is associated with the redox properties of chlorophylls, which may also contribute to the larger population of $P_{D1}^{\bullet+}$ versus $P_{D2}^{\bullet+}$ in PSII.[4−7]

A normal-coordinate structural decomposition (NSD) procedure[10,11] has been developed and used to analyze the nonplanarity of the porphyrin rings, in particular in heme proteins,[12−14] as porphyrin deformations have been widely observed in the high-resolution crystal structures. The NSD approach can describe the character of the out-of-plane distortion observed in the porphyrin geometry, by discriminating the following individual lowest-frequency normal modes: saddling (B_{2u}), ruffling (B_{1u}), doming (A_{2u}), waving [$E_{g(x)}$ and $E_{g(y)}$], and propellering (A_{1u})[10,11] (Figure 2a). In this study, we employed an NSD procedure to characterize the chlorin ring deformations in the 1.9 Å structure of PSII.

COMPUTATIONAL PROCEDURES

As demonstrated in the previous article,[7] we employed the following systematic modeling procedure. First, we constructed a realistic molecular model of the whole PSII complex using the recently determined high-resolution crystal structure. Second, we performed large-scale quantum mechanical/molecular mechanical (QM/MM) calculations for the PSII protein. Finally, using the obtained geometries, we employed an NSD procedure[10,11] to investigate the deformation of the chlorin rings. Technical details of each modeling procedure are summarized below.

Coordinates. The atomic coordinates of PSII were taken from one of two independent but very similar monomers, with chain indicators capitalized, in the X-ray structure of the PSII complexes from *T. vulcanus* at 1.9 Å resolution [Protein Data Bank (PDB) entry 3ARC].[8] Hydrogen atoms were generated and energetically optimized with CHARMM,[15] whereas the positions of all non-hydrogen atoms were fixed. All titratable groups were kept in their standard protonation states; i.e., acidic groups were ionized and basic groups protonated. For

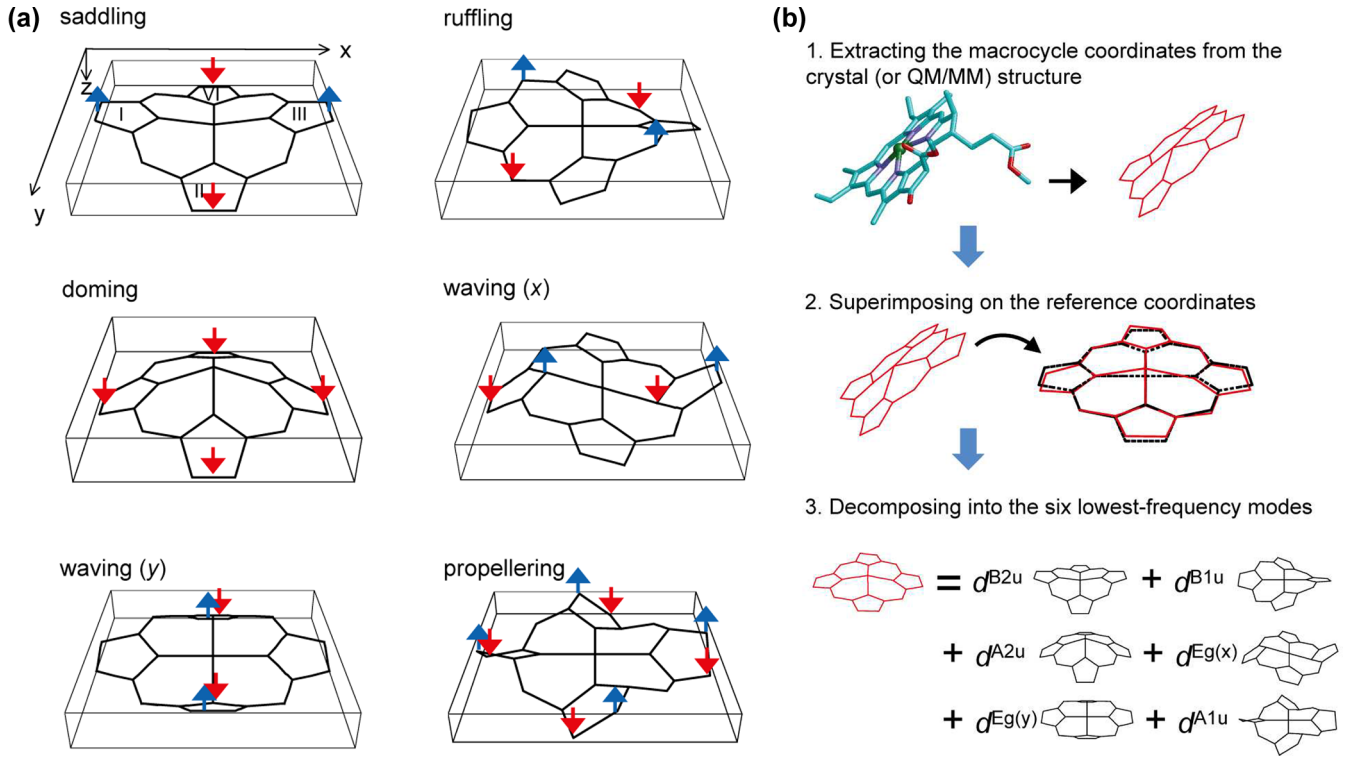

Figure 2. (a) Overviews of the lowest-frequency out-of-plane modes of the porphyrin ring. Red and blue arrows indicate the directions of the motions. (b) NSD analysis was performed in the following steps: (1) extracting the macrocycle coordinates from the crystal (or QM/MM) structure, (2) superimposing the extracted coordinates on the reference coordinates, and (3) decomposing the superimposed coordinates into the reference modes (the six lowest-frequency modes). The reference modes were calculated for the Mg-substituted porphyrin (see Figure S1 of the Supporting Information) with the B3LYP/LACVP* method.

dx.doi.org/10.1021/bi300428s | *Biochemistry* 2012, 51, 4290−4299

the QM/MM calculations, we added additional counterions to neutralize the whole system.

Atomic Partial Charges. Atomic partial charges of the amino acids were adopted from the all-atom CHARMM22[16] parameter set. The atomic charges of the OEC, Chl*a*, Pheo*a*, and quinones were taken from our previous studies of PSII.[7] We considered the OEC as being in state S1 in this study.[7] A mixture of differently reduced S states may cause a change in the net charge of the OEC; however, as described below, the difference in the net charge did not significantly affect our calculated results. The exact valences of the individual Mn atoms are unclear; however, we found that changing the valences of each Mn atom with the same overall charge distribution described above did not significantly affect our calculated results.[7,17]

NSD Analysis. To investigate the out-of-plane distortions of chlorin rings, we employed an NSD procedure with the minimal basis approximation where the deformation profile can be represented by the six lowest-frequency normal modes: saddling (B_{2u}), ruffling (B_{1u}), doming (A_{2u}), waving [$E_{g(x)}$ and $E_{g(y)}$], and propellering (A_{1u}).[10,11] The NSD analysis was performed in three steps (Figure 2b). First, the atomic coordinates of the Mg-substituted macrocycle were extracted from the crystal (or QM/MM-optimized) structure. Second, the extracted coordinates were superimposed on the reference coordinates of the macrocycle (Figure S1 and Table S1a of the Supporting Information). The superimposition is based on a least-squares method, and the mathematical procedure is described in ref 11. Finally, the out-of-plane distortion in the superimposed coordinates was decomposed into the six lowest-frequency normal modes (see Reference Normal Mode Calculation) by the projection to the reference normal mode coordinates as

$$d^{\Gamma} = \sum_{i=1}^{N} \Delta z_i (n_z^{\Gamma})_i \qquad (1)$$

where d^{Γ} represents the distortion component of mode Γ [i.e., $\Gamma = B_{2u}$, B_{1u}, A_{2u}, $E_{g(x)}$, $E_{g(y)}$, or A_{1u}], Δz_i is the z component of superimposed coordinates in the ith heavy atom, and $(n_z^{\Gamma})_i$ is the z component of the normalized eigenvector of reference normal mode Γ in the ith heavy atom. N represents the number of heavy atoms.

Reference Normal Mode Calculation. In previous NSD studies of Chl*a*,[18] a porphyrin was used for the calculation of reference normal modes. In this study, we improved the previous normal mode calculation in two ways.

QM Calculation. In previous studies,[10,11] the normal modes were calculated using a MM approach with a force field parameter set. In this study, we recalculated the normal modes using a QM approach with the DFT/B3LYP functional and LACVP*, which is significantly accurate for describing the electronic properties in comparison with the MM approach. We performed QM calculations with the Jaguar program code.[19]

Consideration of the Mg Ion. In previous studies,[10,11] the porphyrin metal ion was not included in the normal mode calculations. In this study, we included the Mg ion to examine the contribution of the Mg ion position to the resulting modes in response to the axial ligand replacement. We considered the Mg-substituted porphyrin as a reference model (Figure S1 of the Supporting Information). The calculated eigenvectors for the six lowest-frequency reference modes are listed in Table S1b of the Supporting Information.

QM/MM Calculations. QM/MM calculations are not necessarily required for the NSD approach. In this study, we used the QM/MM-optimized geometries mainly to generate the atomic coordinates of Ala-substituted PSII proteins (e.g., D1-H198A and D2-W191A). In doing so, we can calculate the deformation modes of the Ala-substituted PSII, compare the results with those of the native PSII, and clarify the influence of the key side chain on the chlorin deformation modes in native PSII. In all QM/MM calculations reported here, we employed the so-called electrostatic embedding QM/MM scheme and used the Qsite[20] program code. Electrostatic as well as steric effects created by complex PSII architecture were explicitly considered in all of the calculations. Because of the large system size of PSII, the QM region was limited to a particular Chl*a* molecule under question, while other protein units, all cofactors, and water molecules were approximated by the MM force field. We employed the restricted DFT method to describe the closed-shell electronic structure and the unrestricted DFT method for the open-shell electronic structure with the B3LYP functional and LACVP* basis sets. The detailed geometry of Chl*a* was refined by the constrained QM/MM optimizations; the heavy atom coordinates of the surrounding MM region were exactly fixed with the original X-ray coordinates. A Chl*a* monomer (e.g., P_{D1}) and water ligands of Chl_{D2} were defined as the QM region. The results essentially did not change even when the entire P_{D1}/P_{D2} Chl*a* pair was defined as in the QM region (Table S2a of the Supporting Information). In addition, we also confirmed that results did not depend on the functional and the basis in the DFT calculation (Table S2b of the Supporting Information), which justifies the B3LYP/LACVP* method employed in our calculation.

RESULTS AND DISCUSSION

Chlorin Ring Deformation and Associated Modes in the Model System. A model chlorin ring [Chl_{model} (Figure 3, right)] without an axial ligand in vacuum is essentially planar as observed from the absence of each deformation mode (Table 1). Note that Chl_{model} was modeled as the tetrapyrole backbone with a cyclopentanone ring attached to ring III.[21] Upon ligation

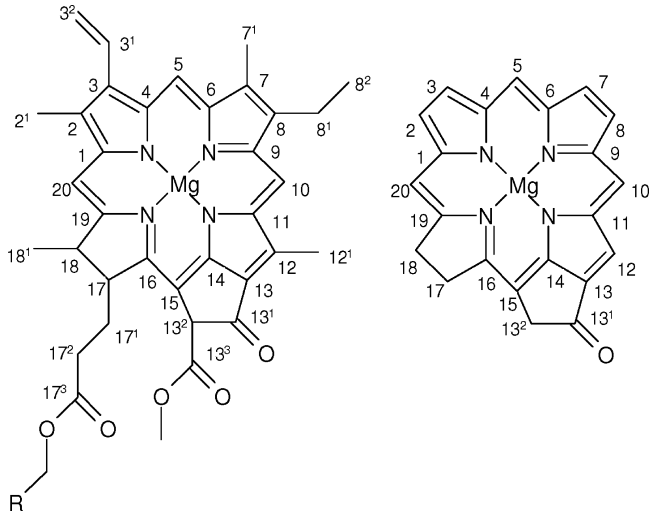

Figure 3. Structure of (left) Chl*a* and (right) Chl_{model}[21] using the IUPAC numbering scheme (R is the phytol chain). The C7═C8 bond in Chl*a* is replaced with a single bond in BChl*a*.

Table 1. Out-of-Plane Distortions (angstroms) of Chl_{model}[21] in the P_{D1}/P_{D2} Pair[a]

		saddling	ruffling	doming	waving		propellering	
		B_{2u}	B_{1u}	A_{2u}	$E_{g(x)}$	$E_{g(y)}$	A_{1u}	total[b]
model	Chl_{model}[c]	0.01	0.06	0.02	0.00	0.00	0.04	0.08
	$[Chl_{model}]^+$[c]	0.01	0.01	0.03	0.00	0.01	0.01	0.04
	$[Chl_{model}]^-$[c]	0.00	**0.14**	0.01	−0.02	−0.02	**0.09**	**0.16**
with His	Chl_{model}[c]	−0.01	0.05	**0.53**	0.00	0.04	0.03	**0.53**
with His	$[Chl_{model}]^+$[c]	−0.02	0.01	**0.71**	0.00	0.05	−0.01	**0.71**
with His	$[Chl_{model}]^-$[c]	0.03	**0.12**	**0.34**	0.00	0.03	**0.08**	**0.37**

[a]Characteristic values relative to the native PSII are shown in bold. For atomic coordinates of the QM-optimized geometries, see the PDB file in the Supporting Information. [b]$\{(B_{1u})^2 + (B_{2u})^2 + (A_{2u})^2 + [E_{g(x)}]^2 + [E_{g(y)}]^2 + (A_{1u})^2\}^{0.5}$. [c]Chlorin ring in Figure 3 (right) without phytol, methyl ester, vinyl, methyl, and ethyl groups.[21]

Table 2. Out-of-Plane Distortions (angstroms) in the Original 1.9 Å Structure (PDB entry 3ARC) and the QM/MM-Optimized Geometry (QM/MM) in the Four-Reaction Center Chl*a* (i.e., P_{D1}, P_{D2}, Chl_{D1}, and Chl_{D2}) in the PSII Protein Environment[a]

		saddling	ruffling	doming	waving		propellering	
		B_{2u}	B_{1u}	A_{2u}	$E_{g(x)}$	$E_{g(y)}$	A_{1u}	total[b]
original 3ARC	P_{D1}	−0.04	**0.45**	**0.60**	−0.01	−0.08	0.12	0.77
QM/MM								
native	P_{D1}	0.20	0.27	0.67	−0.11	0.09	0.16	0.78
	$P_{D1}^{\bullet+}$	0.19	0.29	0.68	0.02	0.14	0.15	0.79
D1-H198A	P_{D1}	0.24	0.26	**0.52**	−0.09	0.10	0.16	**0.66**
original 3ARC	P_{D2}	**-0.64**	0.17	0.28	−0.19	0.00	0.11	0.75
QM/MM								
native	P_{D2}	−0.56	−0.02	0.37	−0.25	0.11	0.16	0.75
	$P_{D2}^{\bullet+}$	−0.57	−0.01	0.38	0.11	0.25	0.16	0.76
D2-H197A	P_{D2}	−0.56	−0.06	**0.04**	−0.24	0.04	0.15	**0.64**
D2-W191A	P_{D2}	**−0.48**	0.03	0.36	−0.21	0.11	0.15	**0.67**
D2-H197A/D2-W191A	P_{D2}	**−0.49**	0.01	**0.11**	−0.18	0.06	0.15	**0.56**
original 3ARC	Chl_{D1}	0.20	**0.40**	0.26	−0.18	0.02	0.16	0.57
QM/MM								
native	Chl_{D1}	0.28	0.43	0.32	−0.16	0.00	0.19	0.65
two H_2O deleted[c]	Chl_{D1}	0.31	0.43	**0.04**	−0.15	0.03	0.20	**0.59**
D1-T179A	Chl_{D1}	0.26	0.49	0.30	−0.13	0.00	0.20	0.67
original 3ARC	Chl_{D2}	**0.39**	−0.02	0.28	−0.21	−0.12	0.11	0.55
QM/MM								
native	Chl_{D2}	0.45	0.01	0.31	−0.17	−0.15	0.14	0.61
two H_2O deleted[d]	Chl_{D2}	0.50	0.00	**0.09**	−0.16	−0.11	0.15	0.56
D2-I178A	Chl_{D2}	0.45	0.04	0.34	−0.13	−0.15	0.15	0.62

[a]Characteristic values in bold. For atomic coordinates of the QM-optimized geometries, see the PDB file in the Supporting Information. [b]$\{(B_{1u})^2 + (B_{2u})^2 + (A_{2u})^2 + [E_{g(x)}]^2 + [E_{g(y)}]^2 + (A_{1u})^2\}^{0.5}$. [c]A ligand water ($H_2O$-1003) and the adjacent water (H_2O-424) were deleted. [d]A ligand water (H_2O-1009) and the adjacent water (H_2O-359) were deleted.

of the His axial ligand, doming of Chl_{model} was induced, resulting in a total displacement of ∼0.5 Å (Table 1). The doming mode in oxidized His-ligated Chl_{model} was further upshifted to ∼0.7 Å, but downshifted to ∼0.3 Å in reduced His-ligated Chl_{model}. On the other hand, small ruffling of Chl_{model} was observed upon reduction, irrespective of the presence or absence of the axial ligand (Table 1). It has been suggested that nonplanar porphyrins are easier to oxidize and harder to reduce than planar porphyrins.[9,10] In this study, deformation of His-ligated Chl_{model} was predominantly contributed by the doming mode, and the deformation was further enhanced upon oxidation. This suggests that the doming mode can contribute to the stabilization of the oxidized state of the chlorin ring.

Deformation in the P_{D1}/P_{D2} Pair. The character of the out-of-plane distortion of the P_{D1} chlorin ring was described predominantly by a large contribution of the doming mode (Table 2). Replacement of the axial ligand D1-His198 with Ala resulted in a slight decrease in the doming mode and also the total out-of-plane distortion (Table 2). Removing the Chl*a* side chains (e.g., phytol, methyl ester, and vinyl groups) yielded weak effects on the degree of distortion (Table S2c of the Supporting Information). However, when the Chl*a* side chains were removed in the D1-H198A mutant, the total out-of-place distortion was largely decreased (Figure 4 and Table S2d of the Supporting Information), although there were still some degrees of distortion. Thus, the deformation modes of P_{D1} were caused by D1-His198, the Chl*a* side chains, and the protein environment of PSII.

The total out-of-plane distortion of P_{D2} was almost identical to that of P_{D1} [∼0.8 Å (Table 2)]. However, its deformation character was significantly different from that of P_{D1}. The mode contributing the most to the P_{D2} deformation was the saddling mode (0.56 Å) rather than the doming mode (0.37 Å). This may partly contribute to the asymmetry in the properties of the P_{D1}/P_{D2} dimer. Upon replacement of the axial ligand D2-His197 with Ala, the doming mode was completely eliminated,

dx.doi.org/10.1021/bi300428s | *Biochemistry* 2012, 51, 4290−4299

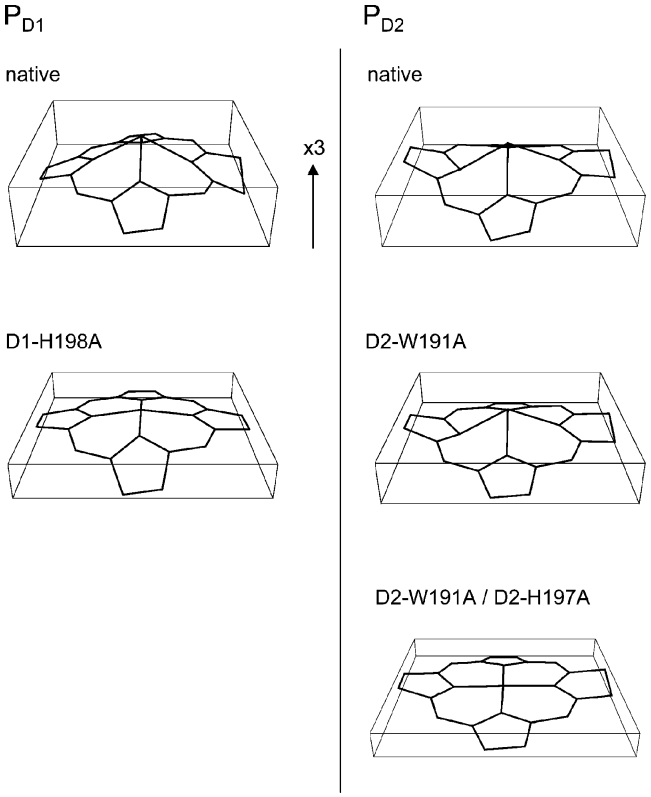

Figure 4. Influence of the mutations on the chlorin ring deformation of the QM/MM optimized Chl_{model} in P_{D1} and P_{D2} (see Table S2d of the Supporting Information for detailed data)..

whereas the saddling mode remained unchanged (Table 2). It appeared that D2-Trp191, which is located near D2-His197, was one of the causes for the large saddling mode. Upon substitution of D2-W191 with Ala, the size of the saddling mode was lowered to 0.48 Å, with a concomitant decrease in the total out-of-plane distortion to 0.67 Å (Table 2). In the D2-H197A/D2-W191A mutant of Chl_{model}, the size of the total out-of-plane distortion was significantly reduced to 0.33 Å (Figure 4 and Table S2d of the Supporting Information). Hence, the deformation of the P_{D2} chlorin ring was caused by D2-Trp191, D2-His197, and the Chl*a* side chains, as well as the protein environment of PSII. Note that the P_{D1} and P_{D2} deformations did not essentially change upon the formation of $P_{D1}^{\bullet+}$ and $P_{D2}^{\bullet+}$, respectively (Table 2), in contrast to the model Chl_{model} in vacuum (Table 1). The absence of the deformation modes upon oxidation of Chl*a* in the PSII protein environment implies that the chlorin ring deformations observed in the 1.9 Å structure are largely associated with steric interactions with the local protein environment rather than their redox abilities (discussed later). It is likely that deformed P_{D1} and P_{D2} are already energetically stable because of the steric interaction with the local protein environment and cannot be easily deformed relative to Chl_{model} in vacuum.

Deformations of Chl*a* in the Photosynthetic Reaction Center (RC). The out-of-plane distortion of the P_{D1}/P_{D2} chlorin rings in the QM/MM geometry was almost identical to that of the original 1.9 Å structure[8] (Table 2), demonstrating that the out-of-plane distortions specifically assigned to each of the Chl*a* molecules in the 1.9 Å structure[8] were quite reasonable. Below, we describe the out-of-plane distortion of all Chl*a* molecules on the basis of the original geometry of the 1.9 Å structure.

The out-of-plane distortion profiles of four Chl*a* molecules in the RC [i.e., P_{D1}, P_{D2}, Chl_{D1}, and Chl_{D2} (Figure 1)], where the initial charge separation proceeds, clearly differ between branches D1 and D2 (Figure 5 and Table 2). The following two notable features were found. (i) Ruffling deformations, which involve a chlorin ring twisting about the Mg−N bond, were large (~0.4 Å) in P_{D1} and Chl_{D1} but apparently smaller in P_{D2} and Chl_{D2}. (ii) Saddling of the P_{D2} and Chl_{D2} rings was significantly larger (~0.4−0.6 Å) than that of P_{D1} and Chl_{D1}. In addition, P_{D1} was found to have the largest doming mode of distortion among the four RC chlorophylls.

Ruffling. Both ruffling and saddling modes are originally absent in the oxidized or neutral His-ligated Chl_{model} (Table 1), suggesting that ruffling of the P_{D1} and Chl_{D1} rings is induced by the PSII protein environment. This is consistent with the fact that substitution of D1-His198 with Ala or removal of the axial water ligand to Chl_{D1} did not affect the degree of ruffling of P_{D1} or Chl_{D1}, respectively (Table 2). In heme protein nitrophorin 4, a ruffling heme deformation was due to the presence of a distal Leu residue, suggesting a significant distal ligand dependence of the ruffling deformation.[13] In cytochrome c_3, it was reported that ruffling of heme, rather than saddling, was strongly associated with a decrease in the redox potential.[12] Recent nuclear magnetic resonance studies of cytochrome c_{552} also suggested that ruffling of heme contributed to the decrease in the redox potential.[14] The apparently large ruffling in P_{D1} and Chl_{D1} relative to that in P_{D2} and Chl_{D2} might be associated with the lower redox potentials in branch D1 versus those in branch D2; this is consistent with formation of (i) the initial intermediate $Chl_{D1}^{\bullet+}Pheo_{D1}^{\bullet-}$ state[1−3] and (ii) the subsequent $P_{D1}^{\bullet+}/P_{D2}^{\bullet+}$ state with a $P_{D1}^{\bullet+}/P_{D2}^{\bullet+}$ ratio of ~80/20,[4−7] where the positive hole is predominately generated and localized in branch D1 upon electronic excitation of P680.

Doming. P_{D1} possessed the largest doming mode (~0.6 Å) among the four Chl*a* molecules in the RC (Figure 5 and Table 2). As doming of the His-ligated Chl_{model} is enhanced upon oxidation (Table 1), large doming of the chlorin ring is probably associated with stabilization of the cationic state. Thus, the largest doming of P_{D1} may be related to its ability to form the cationic state. Together with the ruffling mode, the doming mode of P_{D1} may contribute to the larger $P_{D1}^{\bullet+}$ population[4−7] in the $[P_{D1}/P_{D2}]^{\bullet+}$ state.

Contribution of the Chlorin Ring Deformations to the Redox Potential. It is clear that deformations of porphyrin or chlorin rings, in particular the doming mode, are pronounced as judged by the redox state changes (Table 1). However, recent NSD studies also pointed out that in most cases, the contribution of the porphyrin deformation to the redox potential may not be large.[22] Indeed, a number of NSD studies imply a link between porphyrin deformations and the redox potentials in each heme protein for many years,[12,14] but so far, the heme redox potential values in the protein environment cannot be quantitatively estimated solely from the deformation modes, suggesting that there are other important factors that contribute to the redox potential values in the protein environment.

In previous studies, we demonstrated that the $P_{D1}^{\bullet+}/P_{D2}^{\bullet+}$ ratio (or corresponding spin density distribution) of 80/20[4,5] in the PSII protein environment is predominantly determined by the difference in redox potential between P_{D1} and P_{D2}.[7] The reason for the asymmetric distribution of the cationic state

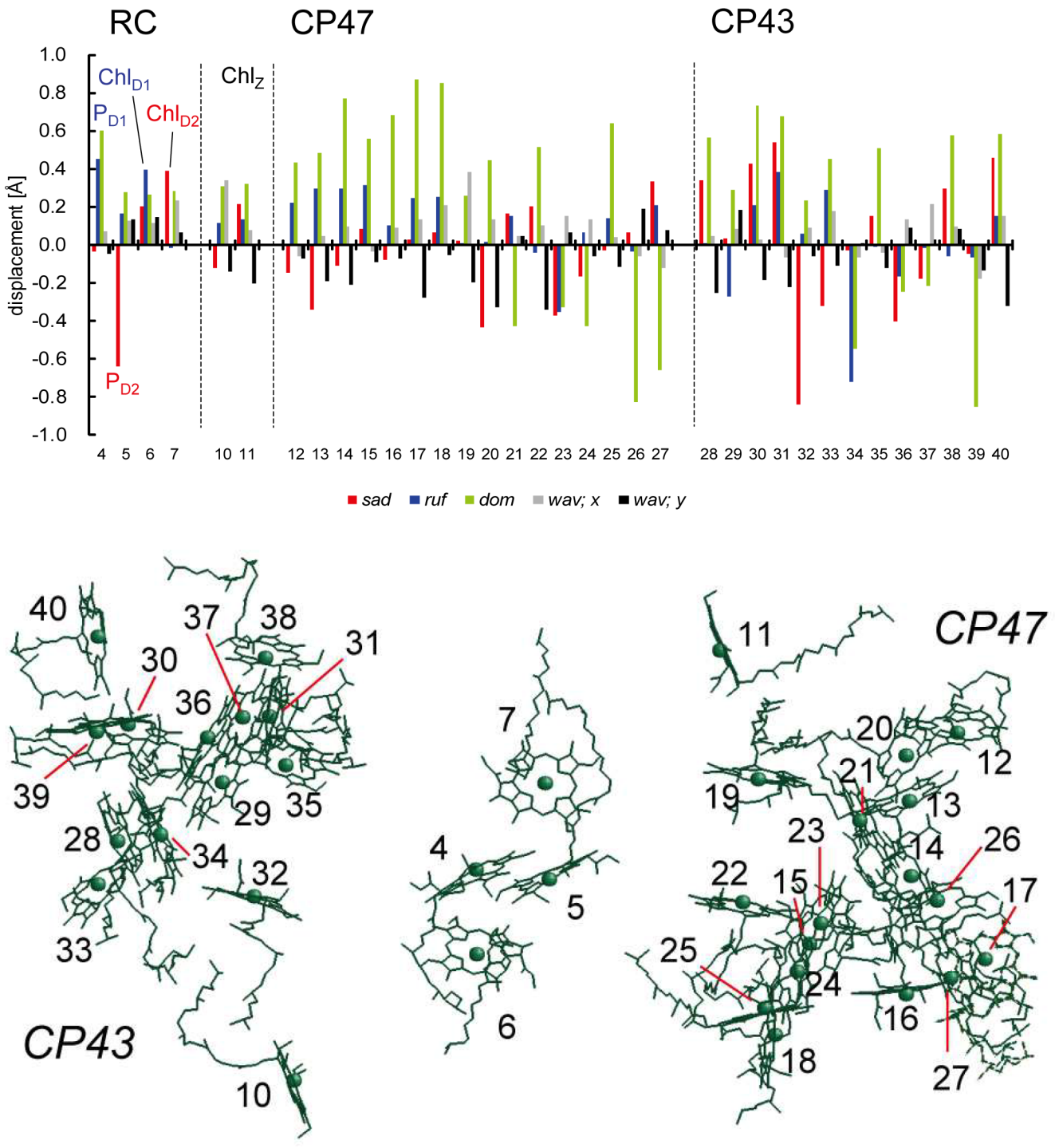

Figure 5. Out-of-plane distortions (vertical axis) of all Chl*a* in the 1.9 Å structure (top). The numbering of the horizontal axis corresponds to the numbering of Chl*a* as presented in the 1.9 Å structure. Overview of the location of Chl*a* in CP47 and CP43 (bottom).

appears to be largely due to differences in several D1/D2 residue pairs, namely, D1-Asn181/D2-Arg180, D1-Asn298/D2-Arg294, D1-Asp61/D2-His61, D1-Glu189/D2-Phe188, and D1-Asp170/D2-Phe169. These residue pairs were responsible for the $P_{D1}^{\bullet+}/P_{D2}^{\bullet+}$ ratio quantum chemically and the difference in redox potential between P_{D1} and P_{D2} electrostatically.[7] Notably, the $P_{D1}^{\bullet+}/P_{D2}^{\bullet+}$ ratio calculated for the P_{D1}/P_{D2} pair (optimized in the PSII protein environment) was nearly 50/50 in the absence of the protein environment[7] irrespective of the characteristic doming and saddling modes being present in P_{D1} and P_{D2}, respectively. This strongly suggests that the influence of the chlorin ring deformations on the redox potentials of P_{D1} and P_{D2} is significantly small with respect to the electrostatic influence of the protein environment. In this study, we also calculated the difference in the ionization energy between deformed Chl_{model} (Table S2d of the Supporting Information) and plainer Chl_{model} (Table 1). The ionization energies of the deformed Chl_{model} types were only 21.9 and 22.1 meV lower than those of the planar Chl_{model} for P_{D1} and P_{D2}, respectively, which is consistent with the previous results.[7]

dx.doi.org/10.1021/bi300428s | *Biochemistry* 2012, 51, 4290−4299

Table 3. Out-of-Plane Distortion (angstroms) of All Chl*a* Molecules in the Original 1.9 Å Structure[a]

				saddling	ruffling	doming	waving		propellering		
	Chl	ligand	B_{2u}	B_{1u}	A_{2u}	$E_{g(x)}$	$E_{g(y)}$	A_{1u}	total[b]	
RC										
P_{D1}	604	D1-H198	−0.04	**0.45**	**0.60**	−0.01	−0.08	0.12	**0.77**	
P_{D2}	605	D2-H197	**−0.64**	0.17	0.28	−0.19	0.00	0.11	**0.75**	
Chl_{D1}	606	H_2O-1003	0.20	**0.40**	0.26	−0.18	0.02	0.16	0.57	
Chl_{D2}	607	H_2O-1009	**0.39**	−0.02	0.28	−0.21	−0.12	0.11	0.55	
$Chl_{Z(D1)}$	610	D1-His118	−0.12	0.11	0.31	−0.14	−0.34	0.17	0.54	
$Chl_{Z(D2)}$	611	D2-H117	0.21	0.13	0.32	0.09	−0.20	0.13	0.48	
CP47	612	H_2O-1027	−0.15	0.22	0.43	0.09	−0.01	0.10	0.52	lumen
	613	H201	−0.34	0.30	0.48	0.10	−0.17	0.14	0.70	lumen
	614	H202	−0.11	0.30	0.77	0.08	−0.21	0.17	0.88	lumen
	615	H455	0.08	0.31	0.56	0.09	−0.04	−0.03	0.65	lumen
	616	H100	−0.08	0.10	0.68	−0.01	−0.11	0.09	0.71	lumen
	617	H157	0.03	0.24	0.87	0.10	−0.29	0.05	0.96	lumen
	618	H_2O-1001	0.06	0.25	0.85	−0.11	−0.18	0.11	0.92	lumen
	619	H466	0.02	0.00	0.26	−0.13	−0.41	0.17	0.53	stroma
	620	H216	−0.44	0.02	0.45	0.13	−0.33	0.11	0.73	stroma
	621	H_2O-1007	0.17	0.15	−0.43	−0.07	0.00	0.09	0.50	stroma
	622	H469	0.20	−0.04	0.51	0.17	−0.31	0.08	0.66	stroma
	623	H23	−0.37	−0.35	−0.33	−0.16	−0.06	0.10	0.64	stroma
	624	H26	−0.17	0.06	−0.43	−0.05	−0.14	0.09	0.49	middle
	625	H9	−0.03	0.14	0.64	0.05	−0.11	0.11	0.67	stroma
	626	H142	0.07	−0.04	−0.83	−0.09	0.18	0.03	0.85	stroma
	627	H114	0.33	0.21	−0.66	0.03	0.14	0.07	0.78	stroma
CP43	628	H237	0.34	0.01	0.56	0.15	−0.21	0.07	0.71	lumen
	629	H430	0.04	−0.27	0.29	−0.19	0.07	0.03	0.45	lumen
	630	H118	0.43	0.21	0.73	0.11	−0.15	−0.06	0.89	lumen
	631	H_2O-1004	0.54	0.38	0.67	0.20	−0.11	0.07	0.97	lumen
	632	H441	−0.84	0.06	0.24	−0.02	−0.10	0.04	0.88	stroma
	633	H251	−0.32	0.29	0.45	−0.05	−0.20	0.12	0.67	stroma
	634	H_2O-816	−0.03	−0.72	−0.54	0.04	0.05	−0.04	0.91	stroma
	635	H444	0.15	−0.01	0.51	0.11	−0.06	0.08	0.55	stroma
	636	H53	−0.40	−0.17	−0.25	−0.16	−0.03	0.02	0.53	stroma
	637	H56	−0.18	−0.02	−0.21	−0.17	−0.13	0.10	0.37	middle
	638	N39	0.29	−0.06	0.58	−0.13	−0.01	−0.05	0.67	stroma
	639	H164	−0.05	−0.07	−0.85	0.22	0.03	0.11	0.89	stroma
	640	H132	0.46	0.15	0.58	0.12	−0.34	0.11	0.85	stroma

[a]Characteristic values are shown in bold. [b]$\{(B_{1u})^2 + (B_{2u})^2 + (A_{2u})^2 + [E_{g(x)}]^2 + [E_{g(y)}]^2 + (A_{1u})^2\}^{0.5}$.

Hence, as previously suggested by a $P_{D1}^{\bullet+}/P_{D2}^{\bullet+}$ ratio,[7] obviously the majority of the redox potential shift in the protein environment is determined by the electrostatic environment (e.g., protein charges) or the availability of solvation energy (e.g., protein volume or shape surrounding the cofactor).[23−25] The chlorin ring deformation is probably induced by steric or electrostatic interaction with the protein environment but appears not to be a primary cause of the shift in the redox potential.

Instead, analyzing the chlorin ring deformation modes will be more useful for characterizing the protein steric environment of Chl*a*. It is not surprising that His-ligated Chl*a* possesses a significantly large doming mode as demonstrated in Table 1. On the other hand, the presence of a ruffling mode in P_{D1} and a saddling mode in P_{D2} in addition to the doming mode (Table 2) appears to directly refer to the difference in "the local steric protein environment" (e.g., D2-Trp191 for P_{D2}) rather than the redox potential value. In this sense, the NSD approach can serve as a powerful tool for determining the character of the local protein environment of each Chl*a* systematically [even without performing QM/MM calculations (see below)]. Keeping this in mind, in the next section, we analyze the out-of-plane distortion profiles of Chl*a* molecules in CP43 and CP47 to characterize the difference in the local protein environment between RC and the antenna complexes.

Deformations of Chl*a* in the Antenna Complexes. The out-of-plane distortion profiles of antenna complexes CP47 and CP43 were obviously different from those of the RC (Figure 5). A significantly large size of doming relative to other deformations can be seen in many Chl*a* molecules in CP47 and CP43. Notably, large doming is not necessarily due to the types of the ligation, because the size of the doming mode in His-ligated Chl*a* lies between 0.2 and 0.9 Å in CP47 and CP43, and similar doming modes were found in Chl*a* molecules with H_2O as the ligand instead of His (Table 3).

This feature resembles light-harvesting complex II where the doming mode was the major contribution to deformation of the chlorin rings.[18] As a possible functional role of the chlorin doming, it was proposed to affect the site energy of Chl*a*.[18] Alternatively, the significantly large doming of Chl*a* in CP47 and CP43 may imply that some of these Chl*a* molecules serve as electron−hole transfer pathways in PSII as previously

dx.doi.org/10.1021/bi300428s | *Biochemistry* 2012, 51, 4290−4299

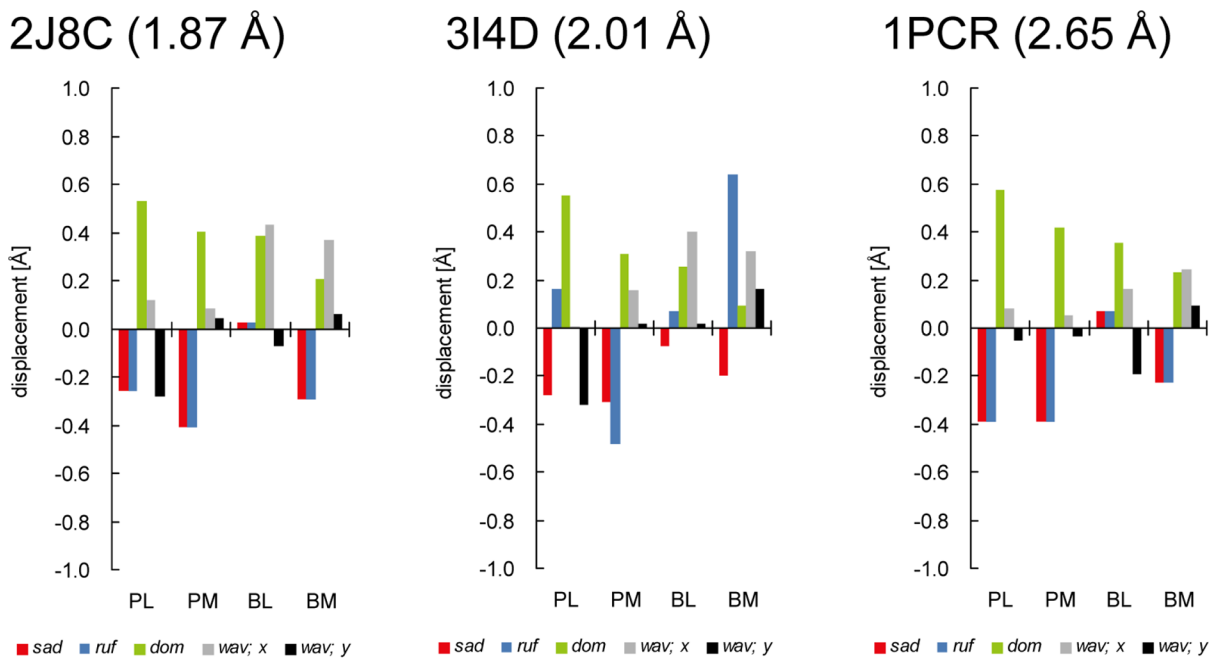

Figure 6. Out-of-plane distortions (vertical axis) of BChl*a* in the crystal structures of PbRC (PDB entries 2J8C, 3I4D, and 1PCR).

proposed;[26] however, such large doming of the chlorin ring was not observed even in the P_{D1}/P_{D2} pair, which can form the $[P_{D1}/P_{D2}]^{\bullet+}$ state.[4−6]

All of the Chl*a* molecules in the RC and a majority of the Chl*a* molecules in CP47 and CP43 possessed positive values in the doming mode (Figure 5). In contrast, five Chl*a* molecules in CP47 (Chl621, -623, -624, -626, and -627) and four Chl*a* molecules in CP43 (Chl634, -636, -637, and -639) possessed negative values in the doming mode, irrespective of the types of axial ligands (His or H_2O). This indicates that the His or H_2O axial ligands are situated on the opposite side of the chlorin plane with respect to the other Chl*a*. These Chl*a* molecules appeared to have a β-configuration, and those Chl*a* molecules with a positive doming mode are in the α-configuration.[27−29] Note that all of these Chl*a* molecules are located on the stromal side or in the middle of the membrane (Table 3). Chl627 (ligand, CP47-His114) was proposed to be the most red-shifted Chl*a* among all Chl*a* molecules in PSII by Raszewski and Renger.[30] Furthermore, the calculated red shifts in the two Chl*a* pairs, Chl623/Chl624 (ligand, CP47-His23/His26) and Chl636/Chl637 (ligand, CP43-His53/His56), were significantly large (~50 cm^{-1}).[30] Thus, β-configuration Chl*a* molecules appeared to play an important role in the excitation energy transfer.[29] Notably, doming modes in the two Chl*a* pairs were smaller than most Chl*a* monomer molecules in CP47 and CP43 (Figure 5), which might be associated with strong excitonic coupling.

In contrast to heme proteins, currently only limited examples are available for deformation of Chl*a*. Further detailed analysis will be needed to understand the functional relevance of the Chl*a* deformation in CP47 and CP43, for instance, as light-harvesting antenna.

Implications of Bacterial Photosynthetic Reaction Centers. The arrangements of the cofactors and the electron transfer pathways in PSII resemble those of photosynthetic reaction centers from purple bacteria (PbRC).[31,32] The four Chl*a* molecules (P_{D1}, P_{D2}, Chl_{D1}, and Chl_{D2}) in PSII correspond to the four bacteriochlorophyll *a* (BChl*a*) molecules (P_L, P_M, B_L, and B_M) in PbRC from *Rhodobacter sphaeroides* (Figure 1). We compared deformations of the four BChl*a* molecules in the three crystal structures of PbRC reported at resolutions of 1.87 Å (PDB entry 2J8C),[33] 2.01 Å (PDB entry 3I4D) (Fjii et al., manuscript to be published), and 2.65 Å (PDB entry 1PCR).[34]

Although there are some discrepancies in deformations of the four BChl*a* molecules among the three structures (e.g., the ruffling mode in B_M is significantly large only in the 2.01 Å structure), a common feature is that P_L displays the largest doming mode among the four BChl*a* molecules in all of the crystal structures investigated (Figure 6). Like the $[P_{D1}/P_{D2}]^{\bullet+}$ state observed in PSII, the $[P_L/P_M]^{\bullet+}$ state can also be observed in PbRC. The $P_L^{\bullet+}$ population is the largest among the four BChl*a* molecules in PbRC (~70/30 $P_L^{\bullet+}/P_M^{\bullet+}$ ratio[35,36]), which also resembles the situation for the $P_{D1}^{\bullet+}$ population among the four Chl*a* molecules in PSII (~80/20 $P_{D1}^{\bullet+}/P_{D2}^{\bullet+}$ ratio[4−7]).

In the absence of the protein environment, the doming mode was induced only upon ligation of the axial ligand (Table 1). In contrast, this appears not to be the case in the PSII protein environment. In PSII, P_{D2} also possesses the His axial ligand, but the doming mode of P_{D2} was much smaller than that of P_{D1} (Figure 5). Via elimination of the axial ligand, the doming mode (0.52 Å) was still present in P_{D1}, whereas those of P_{D2}, Chl_{D1}, and Chl_{D2} were essentially absent (Table 2); this suggests that doming of P_{D1} is caused by the presence of not only D1-His198 but also the other protein environment. The significant contribution of the other protein environment is also the case in the largest doming of P_L in PbRC (Figure 6), because the four BChl*a* molecules possess the His axial ligand. Hence, the largest doming mode and the largest cationic state population in both P_{D1} and P_L may not be a coincidence, possibly arising from common structural features, which should be clarified in future studies.

dx.doi.org/10.1021/bi300428s | *Biochemistry* 2012, 51, 4290−4299

CONCLUSIONS

We investigated the chlorin ring deformations in the 1.9 Å structure, using an NSD procedure. Upon oxidation, the doming mode in His-ligated Chl_{model} was enhanced, suggesting that doming of the chlorin ring can stabilize the oxidized state (Table 1). Deformation of the P_{D1} chlorin ring was mainly due to the large doming mode arising not only from the axial ligand, D1-His198, but also from the Chl*a* side chains and PSII protein environments, whereas deformation of P_{D2} was due to the saddling mode arising from D2-Trp191 and the doming mode arising from D2-His197. Thus, the asymmetry in the property and function of the P_{D1}/P_{D2} pair may partly be caused by the difference in the contributing deformation modes.

Large ruffling was present in P_{D1} and Chl_{D1} but absent in P_{D2} and Chl_{D2}. Because heme ruffling was suggested to contribute to deceasing the heme redox potential in heme proteins,[12,14] ruffling of P_{D1} and Chl_{D1} may also facilitate the formation of the cationic state in branch D1 rather than branch D2, i.e., $P_{D1}^{\bullet+}$[4−7] or $Chl_{D1}^{\bullet+}$.[1−3] Deformations of Chl*a* in RC were in contrast to deformations of Chl*a* in CP47 and CP43, where significantly large doming modes were found in many of the Chl*a* molecules.

In addition to the ruffling mode, P_{D1} possesses the largest doming mode among the four RC Chl*a* molecules, which may further promote the preferential localization of the cationic state in P_{D1} rather than P_{D2} (i.e., the $[P_{D1}/P_{D2}]^{\bullet+}$ state with an ∼80/20 $P_{D1}^{\bullet+}/P_{D2}^{\bullet+}$ ratio[4−7]). This feature also holds true for PbRC, as P_L possessed the largest doming mode (Figure 6) and the population of $P_L^{\bullet+}$ is larger than that of $P_M^{\bullet+}$ (∼70/30 $P_L^{\bullet+}/P_M^{\bullet+}$ ratio[35,36]).

However, the majority of the redox potential shift in the protein environment is determined by the electrostatic environment (e.g., protein charges) or the availability of solvation energy (e.g., protein volume or shape surrounding the cofactor), as previously suggested in a $P_{D1}^{\bullet+}/P_{D2}^{\bullet+}$ ratio.[7] The difference in the chlorin ring deformation appears to directly refer to the difference in "the local steric protein environment" rather than the redox potential in PSII.

ASSOCIATED CONTENT

Supporting Information

Atomic charges, optimized geometries, and computational results of the model systems. This material is available free of charge via the Internet at http://pubs.acs.org.

AUTHOR INFORMATION

Corresponding Author

*Address: 202 Building E, Career-Path Promotion Unit for Young Life Scientists, Graduate School of Medicine, Kyoto University, Yoshida-Konoe-cho, Sakyo-ku, Kyoto 606-8501, Japan. Telephone: +81-75-753-9286. Fax: +81-75-753-9286. E-mail: hiro@cp.kyoto-u.ac.jp.

Funding

This research was supported by the JST PRESTO program (Y.U. and H.I.), a Grant-in-Aid for Scientific Research from the Ministry of Education, Culture, Sports, Science and Technology (MEXT) of Japan (21770163 to H.I. and 22740276 to K.S.), Special Coordination Fund (H.I.) for Promoting Science and Technology of MEXT, the Takeda Science Foundation (H.I.), a Kyoto University Step-up Grant-in-Aid for young scientists (H.I.), and a Grant for Basic Science Research Projects from The Sumitomo Foundation (H.I.).

Notes

The authors declare no competing financial interest.

ACKNOWLEDGMENTS

We thank Dr. Minoru Kubo (University of Hyogo, Hyogo, Japan) for valuable discussions.

ABBREVIATIONS

BChl, bacteriochlorophyll; Chl, chlorophyll; NSD, normal-coordinate structural decomposition; OEC, oxygen-evolving complex; PbRC, photosynthetic reaction centers from purple bacteria; Pheo, pheophytin; PSII, Photosystem II; QM/MM, quantum mechanical/molecular mechanical; RC, photosynthetic reaction center.

REFERENCES

(1) Prokhorenko, V. I., and Holzwarth, A. R. (2000) Primary process and structure of the photosystem II reaction center: A photon echo study. *J. Phys. Chem. B 104*, 11563−11578.

(2) Diner, B. A., and Rappaport, F. (2002) Structure dynamics, and energetics of the primary photochemistry of photosystem II of oxygenic photosynthesis. *Annu. Rev. Plant Biol. 53*, 551−580.

(3) Renger, G., and Renger, T. (2008) Photosystem II: The machinery of photosynthetic water splitting. *Photosynth. Res. 98*, 53−80.

(4) Rigby, S. E. J., Nugent, J. H. A., and O'Malley, P. J. (1994) ENDOR and special triple resonance studies of chlorophyll cation radicals in photosystem 2. *Biochemistry 33*, 10043−10050.

(5) Diner, B. A., Schlodder, E., Nixon, P. J., Coleman, W. J., Rappaport, F., Lavergne, J., Vermaas, W. F. J., and Chisholm, D. A. (2001) Site-directed mutations at D1-His198 and D2-His197 of photosystem II in *Synechocystis* PCC 6803: Sites of primary charge separation and cation and triplet stabilization. *Biochemistry 40*, 9265−9281.

(6) Okubo, T., Tomo, T., Sugiura, M., and Noguchi, T. (2007) Perturbation of the structure of P680 and the charge distribution on its radical cation in isolated reaction center complexes of photosystem II as revealed by Fourier transform infrared spectroscopy. *Biochemistry 46*, 4390−4397.

(7) Saito, K., Ishida, T., Sugiura, M., Kawakami, K., Umena, Y., Kamiya, N., Shen, J.-R., and Ishikita, H. (2011) Distribution of the cationic state over the chlorophyll pair of photosystem II reaction center. *J. Am. Chem. Soc. 133*, 14379−14388.

(8) Umena, Y., Kawakami, K., Shen, J.-R., and Kamiya, N. (2011) Crystal structure of oxygen-evolving photosystem II at 1.9 Å resolution. *Nature 473*, 55−60.

(9) Barkigia, K. M., Chantranupong, L., Smith, K. M., and Fajer, J. (1988) Structural and theoretical models of photosynthetic chromophores. Implications for redox, light-absorption properties and vectorial electron flow. *J. Am. Chem. Soc. 110*, 7566−7567.

(10) Shelnutt, J. A., Song, X.-Z., Ma, J.-G., Jia, S.-L., Jentzen, W., and Medforth, C. J. (1998) Nonplanar porphyrins and their significance in proteins. *Chem. Soc. Rev. 27*, 31−41.

(11) Jentzen, W., Song, X.-Z., and Shelnutt, J. A. (1997) Structural characterization of synthetic and protein-bound porphyrins in terms of the lowest-frequency normal coordinates of the macrocycle. *J. Phys. Chem. B 101*, 1684−1699.

(12) Ma, J. G., Zhang, J., Franco, R., Jia, S. L., Moura, I., Moura, J. J., Kroneck, P. M., and Shelnutt, J. A. (1998) The structural origin of nonplanar heme distortions in tetraheme ferricytochromes c_3. *Biochemistry 37*, 12431−12442.

(13) Kubo, M., Gruia, F., Benabbas, A., Barabanschikov, A., Montfort, W. R., Maes, E. M., and Champion, P. M. (2008) Low-frequency mode activity of heme: Femtosecond coherence spectroscopy of iron porphine halides and nitrophorin. *J. Am. Chem. Soc. 130*, 9800−9811.

(14) Liptak, M. D., Wen, X., and Bren, K. L. (2010) NMR and DFT investigation of heme ruffling: Functional implications for cytochrome *c*. *J. Am. Chem. Soc. 132*, 9753−9763.
(15) Brooks, B. R., Bruccoleri, R. E., Olafson, B. D., States, D. J., Swaminathan, S., and Karplus, M. (1983) CHARMM: A program for macromolecular energy minimization and dynamics calculations. *J. Comput. Chem. 4*, 187−217.
(16) MacKerell, A. D., Jr., Bashford, D., Bellott, R. L., Dunbrack, R. L., Jr., Evanseck, J. D., Field, M. J., Fischer, S., Gao, J., Guo, H., Ha, S., Joseph-McCarthy, D., Kuchnir, L., Kuczera, K., Lau, F. T. K., Mattos, C., Michnick, S., Ngo, T., Nguyen, D. T., Prodhom, B., Reiher, W. E., III, Roux, B., Schlenkrich, M., Smith, J. C., Stote, R., Straub, J., Watanabe, M., Wiorkiewicz-Kuczera, J., Yin, D., and Karplus, M. (1998) All-atom empirical potential for molecular modeling and dynamics studies of proteins. *J. Phys. Chem. B 102*, 3586−3616.
(17) Saito, K., Shen, J.-R., Ishida, T., and Ishikita, H. (2011) Short hydrogen-bond between redox-active tyrosine Y_Z and D1-His190 in the photosystem II crystal structure. *Biochemistry 50*, 9836−9844.
(18) Zucchelli, G., Brogioli, D., Casazza, A. P., Garlaschi, F. M., and Jennings, R. C. (2007) Chlorophyll ring deformation modulates Qy electronic energy in chlorophyll-protein complexes and generates spectral forms. *Biophys. J. 93*, 2240−2254.
(19) *Jaguar*, version 7.5 (2008) Schrödinger, LLC, New York.
(20) *QSite*, version 5.6 (2010) Schrödinger, LLC, New York.
(21) Heimdal, J., Jensen, K. P., Devarajan, A., and Ryde, U. (2007) The role of axial ligands for the structure and function of chlorophylls. *J. Biol. Inorg. Chem. 12*, 49−61.
(22) Karunakaran, V., Denisov, I., Sligar, S. G., and Champion, P. M. (2011) Investigation of the low frequency dynamics of heme proteins: Native and mutant cytochrome $P450_{cam}$ and redox partner complexes. *J. Phys. Chem. B 115*, 5665−5677.
(23) Voigt, P., and Knapp, E. W. (2003) Tuning heme redox potentials in the cytochrome c subunit of photosynthetic reaction centers. *J. Biol. Chem. 278*, 51993−52001.
(24) Mao, J., Hauser, K., and Gunner, M. R. (2003) How cytochromes with different folds control heme redox potentials. *Biochemistry 42*, 9829−9840.
(25) Ishikita, H., Eger, B. T., Okamoto, K., Nishino, T., and Pai, E. F. (2012) Protein conformational gating of enzymatic activity in xanthine oxidoreductase. *J. Am. Chem. Soc. 134*, 999−1009.
(26) Vasil'ev, S., Brudvig, G. W., and Bruce, D. (2003) The X-ray structure of photosystem II reveals a novel electron transport pathway between P680, cytochrome b559 and the energy-quenching cation, Chl_Z. *FEBS Lett. 543*, 159−163.
(27) Balaban, T. S., Fromme, P., Holzwarth, A. R., Krauss, N., and Prokhorenko, V. I. (2002) Relevance of the diastereotopic ligation of magnesium atoms of chlorophylls in Photosystem I. *Biochim. Biophys. Acta 1556*, 197−207.
(28) Oba, T., and Tamiaki, H. (2002) Which side of the π-macrocycle plane of (bacterio)chlorophylls is favored for binding of the fifth ligand? *Photosynth. Res. 74*, 1−10.
(29) Balaban, T. S., Braun, P., Hattig, C., Hellweg, A., Kern, J., Saenger, W., and Zouni, A. (2009) Preferential pathways for light-trapping involving β-ligated chlorophylls. *Biochim. Biophys. Acta 1787*, 1254−1265.
(30) Raszewski, G., and Renger, T. (2008) Light harvesting in photosystem II core complexes is limited by the transfer to the trap: Can the core complex turn into a photoprotective mode? *J. Am. Chem. Soc. 130*, 4431−4446.
(31) Michel, H., and Deisenhofer, J. (1988) Relevance of the photosynthetic reaction center from purple bacteria to the structure of photosystem II. *Biochemistry 27*, 1−7.
(32) Rutherford, A. W., and Faller, P. (2003) Photosystem II: Evolutionary perspectives. *Philos. Trans. R. Soc. London, Ser. B 358*, 245−253.
(33) Koepke, J., Krammer, E. M., Klingen, A. R., Sebban, P., Ullmann, G. M., and Fritzsch, G. (2007) pH modulates the quinone position in the photosynthetic reaction center from *Rhodobacter sphaeroides* in the neutral and charge separated states. *J. Mol. Biol. 371*, 396−409.
(34) Ermler, U., Fritzsch, G., Buchanan, S. K., and Michel, H. (1994) Structure of the photosynthetic reaction centre from *Rhodobacter sphaeroides* at 2.65 Å resolution. *Structure 2*, 925−936.
(35) Lendzian, F., Huber, M., Isaacson, R. A., Endeward, B., Plato, M., Bönigk, B., Möbius, K., Lubitz, W., and Feher, G. (1993) The electronic structure of the primary donor cation radical in *Rhodobacter sphaeroides* R-26: ENDOR and TRIPLE resonance studies in single crystals of reaction centers. *Biochim. Biophys. Acta 1183*, 139−160.
(36) Muh, F., Lendzian, F., Roy, M., Williams, J. C., Allen, J. P., and Lubitz, W. (2002) Pigment-protein interactions in bacterial reaction centers and their influence on oxidation potential and spin density distribution of the primary donor. *J. Phys. Chem. B 106*, 3226−3236.